# Generation and detection of spin-orbit coupled neutron beams

Dusan Sarenac[a,1], Connor Kapahi[a,b], Wangchun Chen[c,d], Charles W. Clark[e], David G. Cory[a,f,g,h], Michael G. Huber[i], Ivar Taminiau[a], Kirill Zhernenkov[a,j,k], and Dmitry A. Pushin[a,b]

[a]Institute for Quantum Computing, University of Waterloo, Waterloo, ON N2L 3G1, Canada; [b]Department of Physics, University of Waterloo, Waterloo, ON N2L 3G1, Canada; [c]NIST Center for Neutron Research, National Institute of Standards and Technology, Gaithersburg, MD 20899; [d]Department of Materials Science and Engineering, University of Maryland, College Park, MD 20742; [e]Joint Quantum Institute, National Institute of Standards and Technology and University of Maryland, College Park, MD 20742; [f]Department of Chemistry, University of Waterloo, Waterloo, ON N2L 3G1, Canada; [g]Perimeter Institute for Theoretical Physics, Waterloo, ON N2L 2Y5, Canada; [h]Canadian Institute for Advanced Research, Toronto, Ontario M5G 1Z8, Canada; [i]Physical Measurement Laboratory, National Institute of Standards and Technology, Gaithersburg, MD 20899; [j]Jülich Centre for Neutron Science at Heinz Maier-Leibnitz Zentrum, Forschungszentrum Jülich GmbH, 85748 Garching, Germany; and [k]Frank Laboratory of Neutron Physics, Joint Institute for Nuclear Research, 141980 Dubna, Moscow Region, Russia

Edited by Anton Zeilinger, University of Vienna, Vienna, Austria, and approved August 30, 2019 (received for review April 23, 2019)

**Spin-orbit coupling of light has come to the fore in nanooptics and plasmonics, and is a key ingredient of topological photonics and chiral quantum optics. We demonstrate a basic tool for incorporating analogous effects into neutron optics: the generation and detection of neutron beams with coupled spin and orbital angular momentum. The $^3$He neutron spin filters are used in conjunction with specifically oriented triangular coils to prepare neutron beams with lattices of spin-orbit correlations, as demonstrated by their spin-dependent intensity profiles. These correlations can be tailored to particular applications, such as neutron studies of topological materials.**

neutron optics | orbital angular momentum | spin-orbit coupling

Studies of optical orbital angular momentum (OAM) have blossomed since the early 1990s and are now encompassed in a larger framework of structured waves of light and matter (1, 2). OAM has been induced in beams of light (3), electrons (4–6), and neutrons (7). Photonic OAM has demonstrated usefulness in edge-detection microscopy, quantum information processing protocols, encoding and multiplexing of communications, and optical manipulation of matter (8–15). Electron OAM beams have found applications in the characterization of nanoscale magnetic fields in materials (16) and exploration of magnetic monopoles (17). Neutron OAM has shown promise in the detection of buried interfaces (18). Furthermore, it has been theorized that neutron OAM can modify Schwinger scattering of neutrons on nuclei (19), and might also enable studies of neutron's internal structure (20).

A related set of techniques have been developed for preparing and characterizing beams in which the spin and OAM are correlated. In the case of photons, these "spin-orbit" beams possess correlations between polarization and the OAM (21, 22), whereas, for electrons and neutrons, the correlations are between the spin and the OAM (23, 24). Photonic spin-orbit beams have been demonstrated, and they have enriched the application range of OAM beams by increasing the number of accessible degrees of freedom (25–28). Although analogous preparation methods have been proposed for electrons (23, 29–31), they have yet to be implemented in the laboratory.

In this paper, we demonstrate not only the preparation and characterization of spin-orbit beams using neutrons but also neutron beams with a lattice of spin-orbit correlations. Our technique, which we previously demonstrated with light (32), involves the preparation of a spin-orbit textured "lattice of vortices" wavefront. A variety of textures can be generated by this method (33), including skyrmion-like geometries analogous to those recently observed in evanescent electromagnetic fields (34). We expect the techniques shown here to pave the way for neutron OAM and spin-orbit applications in material characterization and fundamental physics.

The setup is composed of a slit, 2 $^3$He neutron spin filters, guide field coils, 2 pairs of specifically orientated triangular coils, a permalloy tube, and a neutron camera. A $1 \times 1$ mm$^2$ slit was placed at the start of the setup. The slit sets the lower limit on the transverse coherence length at the first triangular coil to

$$\sigma = \frac{\lambda L_1}{s} \approx 0.4\ \mu\text{m}, \qquad [1]$$

where $L_1 = 0.965$ m is the distance from the slit to the first triangular coil and $s$ is the slit width. Although it might be desirable for some specific applications to reduce the slit width to the point that the transverse coherence length extends over the beam diameter, it is not practical in this experiment, as the neutron peak count rate was $\sim 15\,\text{s}^{-1}$ at the camera.

Two $^3$He cells were used as the spin polarizer and the spin analyzer, due to their spatially homogeneous neutron polarization (35). The spin filter direction could be aligned with the $\pm z$ axis at the beamline using the adiabatic fast passage nuclear magnetic resonance method (36).

To prepare neutron beams with lattices of spin-orbit correlations, we used specifically orientated triangular coils that acted as "lattice of optical vortices" (LOV) prism pairs (32, 33). They were arranged to induce magnetic phase gradients perpendicular to each other as well as to the incoming neutron beam. Therefore

## Significance

**Extensive interest has been placed on the techniques to prepare and characterize optical and matter wave orbital angular momentum (OAM) beams and spin correlated OAM beams. They have been shown to be useful in a wide range of applications such as microscopy, quantum information processing, material characterization, and communication protocols. Here we demonstrate an observation of spin-orbit beams and lattices of spin-orbit beams with neutrons. Neutrons, which do not possess a charge and have significant mass, are probes of nature that are complementary to photons and electrons. The techniques shown here enable neutron OAM applications in material characterization and fundamental physics.**

Author contributions: D.S., D.G.C., and D.A.P. designed research; C.K., W.C., M.G.H., and K.Z. performed research; D.S., C.K., and D.A.P. analyzed data; D.S., C.K., W.C., C.W.C., D.G.C., M.G.H., I.T., K.Z., and D.A.P. wrote the paper; and D.S., C.K., I.T., K.Z., and D.A.P. designed and built the triangular coils.

The authors declare no conflict of interest.

This article is a PNAS Direct Submission.



[1]To whom correspondence may be addressed. Email: dsarenac@uwaterloo.ca.

the coil arrangement differs from the Wollaston arrangement where 2 triangular coils with antiparallel fields are placed with their inclined sides facing each other (37, 38).

As shown in Fig. 1, there is a spatially dependent path difference between the second and the third triangular coils due to their inclined sides. Therefore, it is necessary to minimize the magnetic field in this region to avoid an unwanted phase gradient across the beam. In our setup, this was accomplished via a permalloy tube. Guide coils were placed between other triangular coils to provide a uniform magnetic field along the spin quantization axis.

The first $^3$He polarizer filters the neutrons with spin along the beam propagation axis, thereby setting the neutron wavefunction to

$$|\Psi_{\text{in}}\rangle = |\uparrow_z\rangle\,. \qquad [2]$$

The triangular coils induce perpendicular phase gradients along the directions that are also perpendicular to the direction of the incoming spin state. Pairs of triangular coils then effectively act as LOV prism pairs, as described in ref. 33. In this particular case, their individual operators are given by

$$\hat{U}_y = e^{-i\frac{\pi}{a}y\hat{\sigma}_x} \qquad \hat{U}_x = e^{-i\frac{\pi}{a}x\hat{\sigma}_y}, \qquad [3]$$

where $\hat{\sigma}_y$ and $\hat{\sigma}_x$ are the Pauli spin operators, and $a$ is the spatial spin oscillation period. For the case of no beam divergence,

$$a = \frac{2\pi v_z}{\gamma_{\text{n}}|B|\tan(\theta)}, \qquad [4]$$

where $|B|$ is the magnetic field inside the triangular coils, $v_z$ is the neutron velocity, $\gamma_{\text{n}}$ is the neutron gyromagnetic ratio (39), and $\theta$ is the incline angle of the triangle coils. For example, for a field of $|B| = 0.005$ T inside the triangular coils, the corresponding period of a nondiverging beam would be $a = 3.8$ mm.

A pair of specifically orientated triangular coils, or a LOV prism pair, approximates the action of a quadrupole magnetic field (32). The state induced by a quadrupole acting on $|\Psi_{\text{in}}\rangle = |\uparrow_z\rangle$ has the following form (24):

$$|\Psi_Q\rangle \approx \left[\cos\left(\frac{2\pi r}{a}\right)|\uparrow_z\rangle + ie^{-i\phi}\sin\left(\frac{2\pi r}{a}\right)|\downarrow_z\rangle\right], \qquad [5]$$

where $(r, \phi)$ are the cylindrical coordinates. It follows from Eq. **5** that 2 spin states possess a differing spatial amplitude profile and that there is an azimuthal phase difference between the 2 spin states which indicates the OAM difference between the 2 spin states of $\Delta\ell = \ell_\uparrow - \ell_\downarrow = 1$.

In addition to approximating the quadrupole operator, LOV prism pairs possess a periodic structure which induces a 2-dimensional lattice structure in the output state (32). The state after $N$ sets of LOV prism pairs is given by

$$|\Psi^N_{\text{LOV}}\rangle = (\hat{U}_x\,\hat{U}_y)^N|\Psi_{\text{in}}\rangle\,. \qquad [6]$$

The small transverse coherence length given by Eq. **1** indicates that we do not have a single eigenstate of OAM in the incoming beam but rather a distribution of OAM states. Therefore, for each lattice cell, if we assume symmetry in the incoming transverse momentum distribution, filtering $|\uparrow_z\rangle$ neutrons would result in an OAM distribution with a mean value of 0, while filtering $|\downarrow_z\rangle$ neutrons would result in an OAM distribution with mean value 1.

## Results and Discussion

After passing through one of the triangular coils, the spin state varies sinusoidally along the direction of the coil incline.

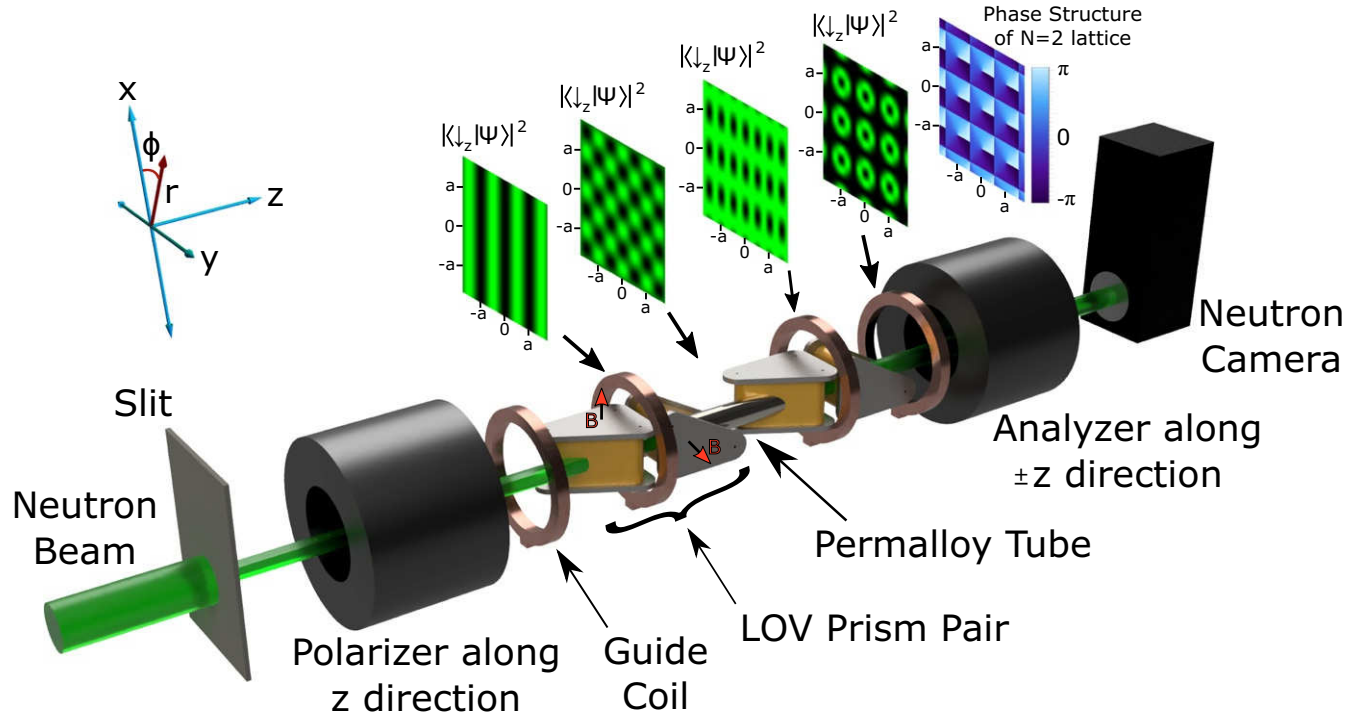


**Fig. 1.** Schematic diagram of the experimental setup which consists of a slit, a $^3$He spin polarizer and analyzer, guide field coils, 2 pairs of specifically oriented triangular coils that act as LOV prism pairs, a permalloy tube, and a neutron camera. The triangular coils induce perpendicular magnetic phase gradients onto the neutron wavefunction. LOV prism pairs prepare beams with a lattice of spin-orbit correlations where, in each lattice cell, the phase between the 2 spin states varies azimuthally. The simulated spin-dependent intensity profile after each triangular coil is shown in green, and the profile of the phase difference between the 2 spin states, given by $(\arg[\langle\downarrow_z|\Psi^{N=2}_{\text{LOV}}\rangle] - \arg[\langle\uparrow_z|\Psi^{N=2}_{\text{LOV}}\rangle])$, is shown in blue.

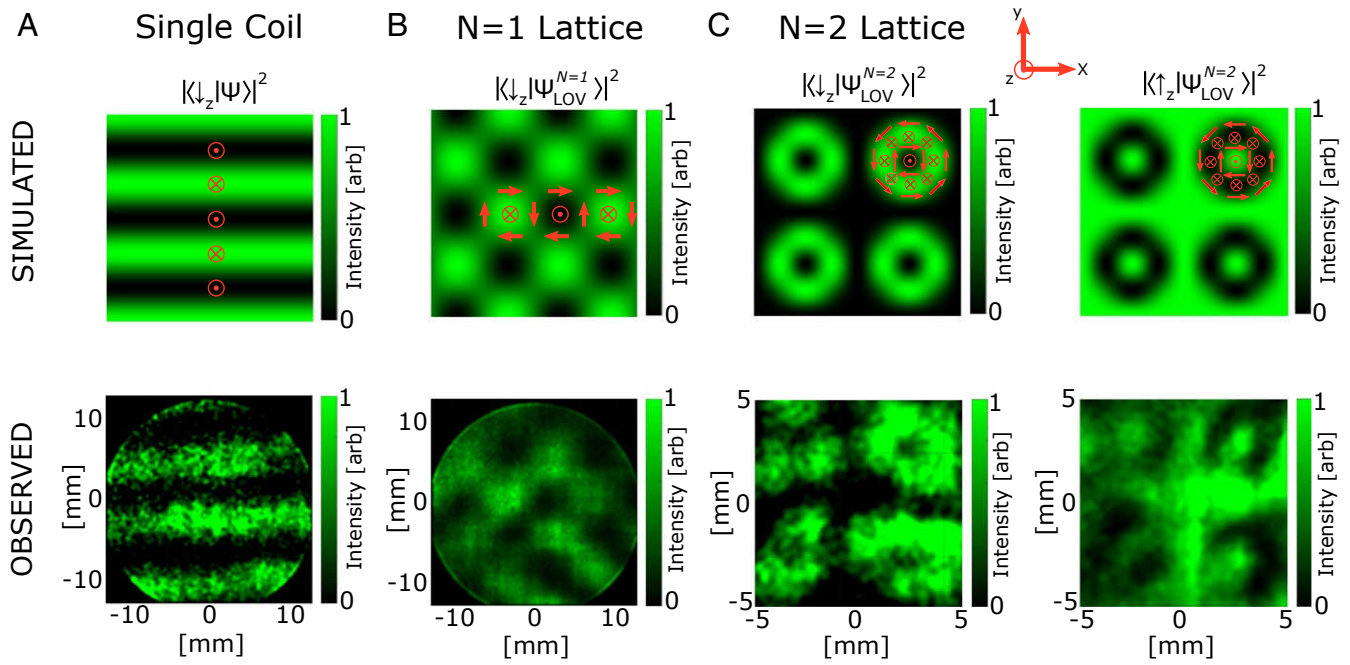


**Fig. 2.** The simulated and observed spin-dependent intensity profiles. A Gaussian filter as well as an intensity gradient was added to each observed image, to highlight the features of interest. The currents on the (first, second, third, and fourth) triangular coil were set to (*A*) (0, 0, 0, and 2.5 A), (*B*) (2.5, 2.5, 0, and 0 A), and (*C*) (5, 5, 5, and 4 A). The spatially varying spin direction (before the spin filtering) is overlaid on the simulated intensity profiles via the red arrows. The N = 1 lattice exhibits a vortex antivortex structure, and its spin-dependent intensity profile resembles a checkerboard pattern. The N = 2 lattice appears as a lattice of doughnut/ring shapes. Good qualitative agreement is shown between the simulated and observed intensity profiles.

Therefore the intensity profile postselected on one spin state exhibits linear fringes with period $a$, as shown in Fig. 2*A*. After passing through a pair of perpendicular triangular coils, or an LOV prism pair, an N = 1 lattice of spin-orbit correlations is prepared. The intensity profile postselected on $|\downarrow_z\rangle$ is shown in Fig. 2*B*, and it resembles a checkerboard pattern. The spin direction before the postselection is overlaid on the intensity profile via the red arrows, and it elucidates why the N = 1 lattice is composed of a vortex antivortex structure.

Passing a polarized neutron beam through 2 pairs of LOV prism pairs prepares a beam with a lattice of spin-orbit correlations as described by Eq. **5**. The spin-dependent intensity profile has the doughnut/ring structure as shown in Fig. 2*C*. This is a consequence of the cosine/sine amplitude terms in Eq. **5**. The major features can be seen between the simulated and observed profiles in Fig. 2*C*. Note that the spin analyzer sets the spin filter direction, and the 2 profiles in Fig. 2*C* are from 2 separate setup configurations.

The slight differences between the simulated and observed profiles shown in Fig. 2 *A* and *B* can be attributed to the interface region between the longitudinal field of the guide coils and the transverse field of the triangular coils. However, when triangular coils 2 and 3 are used to prepare the N = 1 lattice, the observed profile is significantly more distorted, indicating that the permalloy tube is not sufficiently removing the field between the triangular coils. A nonzero magnetic field in the permalloy tube results in a path gradient, due to the inclined sides of the triangular coils. Fig. 3 shows the distortions that arise when a uniform $B_z = 6 \times 10^{-4}$ T magnetic field is present beside the inclined sides of the second and third triangular coils. It can be observed that the doughnut profiles become stretched, and that, therefore, gradients are a possible cause of the distortions that are observed in Fig. 2*C*.

The phase difference between the 2 spin states of the N = 2 lattice is shown in Fig. 1. This phase structure can be mapped via the spin-dependent intensity profile after mixing the 2 spin states. That is, we require postselection of the spin along a direction that is perpendicular to the spin quantization axis, which, in our case, would be the $x$ and $y$ directions.

It can be noted that translating one of the triangular coils along its incline direction induces an additional uniform phase shift. This provides a convenient method of obtaining the $|\downarrow_{x,y}\rangle$-dependent intensity profiles without changing the $^3$He

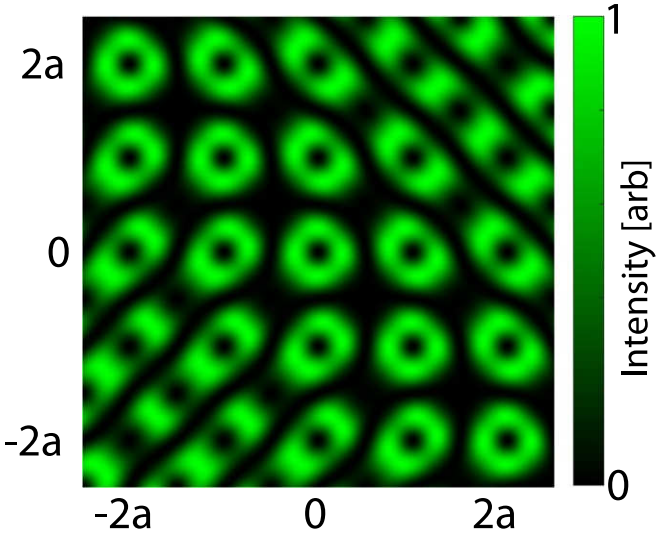


**Fig. 3.** The simulated distortions when including a $B_z = 6 \times 10^{-4}$ T magnetic field beside the inclined sides of the second and third triangular coil. The magnetic field results in a gradient along the negative $y$ direction after the second triangular coil followed by a gradient along the negative $x$ direction before the third triangular coil. It can be observed that gradients are a possible cause of the distortions that are observed in Fig. 2*C*.

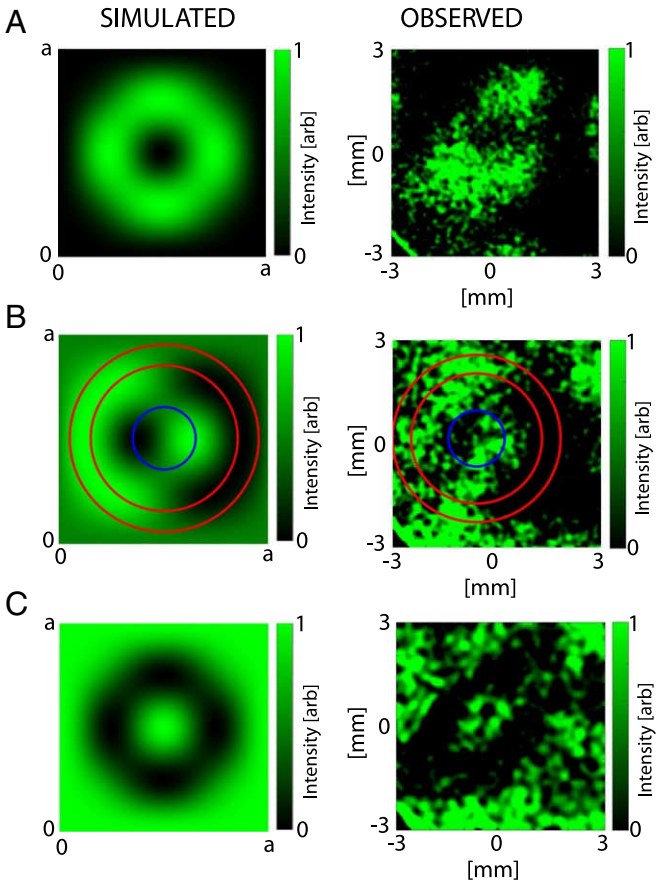


**Fig. 4.** The simulated and observed spin-dependent intensity profile, after 2 sets of LOV prism pairs, as the first coil in the setup is translated along the *y* direction (see Fig. 1) for (*A*) 0, (*B*) 3, and (*C*) 6 mm. The profiles in *A* and *C* correspond to the spin-up and spin-down intensity profiles of a single cell of the N = 2 lattice, as shown in Fig. 2. The profile in *B* corresponds to the intensity profile after mixing the 2 spin states. The 2 regions that manifest out-of-phase azimuthal variation are pictorially bounded by the red and blue circles. It can be seen that the intensity varies azimuthally, indicating the phase structure of a single cell in the N = 2 lattice, as shown in Fig. 1.

polarization direction (33). Fig. 4 shows the simulated and observed spin-dependent intensity profile as the first coil in the setup is translated along the *y* direction. Fig. 4 *A* and *C* corresponds to the spin-up and spin-down intensity profiles of a single cell of the N = 2 lattice, as shown in Fig. 2. Fig. 4*B* corresponds to the intensity profile after mixing the 2 spin states.

To quantify the data shown in Fig. 4*B*, we can consider the 2 regions pictorially bounded by the red and blue circles that manifest out-of-phase azimuthal variation. The inner (outer) region in the simulation profile where the azimuthal variation is found to be the most pronounced is bound by $r = 0$ and $r = 0.15a$ ($r = 0.35a$ and $r = 0.45a$). On the experimental data, the origin was picked to be at the center of the intensity transition, and the period is set to $a = 5.29$ mm. Fig. 5 shows the azimuthal variations in the integrated intensities of the observed image in Fig. 4*B*. The intensity curves were normalized with respect to the area under the curves, and they were constructed by integrating over the radial direction and 10° increments in the azimuthal direction. The fits (dashed lines) were computed from the simulated image of Fig. 4*B*. The one sinusoidal period is a signature of the OAM = 1 phase structure. Longer data acquisition times would be required to increase the signal to noise ratio.

Photon spin-orbit coupling arises naturally in nanooptics, photonics, plasmonics, and optical metamaterials (40, 41) and is a core construct of chiral quantum optics (42) and topological photonics (43). Here we show spin-orbit coupling in the context of freely propagating beams in which spin and OAM degrees of freedom are correlated. We have prepared and characterized neutron beams with lattices of spin-orbit correlations in which the OAM of one spin state is different from the OAM of the other spin state. This was achieved via sets of specifically oriented triangular coils which acted as LOV prism pairs. The beams were characterized via their spin-dependent intensity profiles.

The triangular coils induced good quality magnetic phase gradients, as can be observed in Fig. 2 *A* and *B*. However, in our experiment, the permalloy tube did not sufficiently remove the magnetic field between the 2 sets of triangular coils. This resulted in distortions when all 4 coils were on simultaneously. For more pronounced results, a better mechanism of removing the field is required.

We expect the described techniques to be the forerunners of neutron OAM applications in material characterization and fundamental physics. Superconducting triangular coils with higher fields may be employed to prepare lattices with smaller periods. The next set of experiments will focus on the preparation of spin-orbit correlations over the coherence length of neutron wave packets and the characterization of these spin-orbit states via the correlations between spin and projected linear momentum.

## Materials and Methods

The experiment was carried out on the Polarized $^3$He And Detector Experiment Station (PHADES) (44) at the National Institute for Standards and Technology Center for Neutron Research. A monochromatic beam of neutrons with wavelength $\lambda = 0.41$ nm ($\Delta\lambda/\lambda \approx 2\%$) was directed into the setup, as shown in Fig. 1. The beam divergence was $\sim 1^\circ$ in both *x* and *y* directions. The setup is composed of a slit, 2 $^3$He neutron spin filters, guide field coils, 2 pairs of specifically orientated triangular coils, a permalloy tube, and a neutron camera. The neutron camera has a 25-mm-diameter active area, a spatial resolution of 100 μm, and a quantum efficiency of $\sim 38\%$ (45).

Two $^3$He cells were polarized in an off-line lab using spin-exchange optical pumping (46), and they were changed 3 times during the experiment. Their initial $^3$He polarization at the beamline was measured to be between 73% and 82%, while their relaxation time was measured to be between 365 and 516 h. The polarization of the neutron beam would reduce from $\sim 94$ to $\sim 90\%$ during a 2- to 3-day time period.

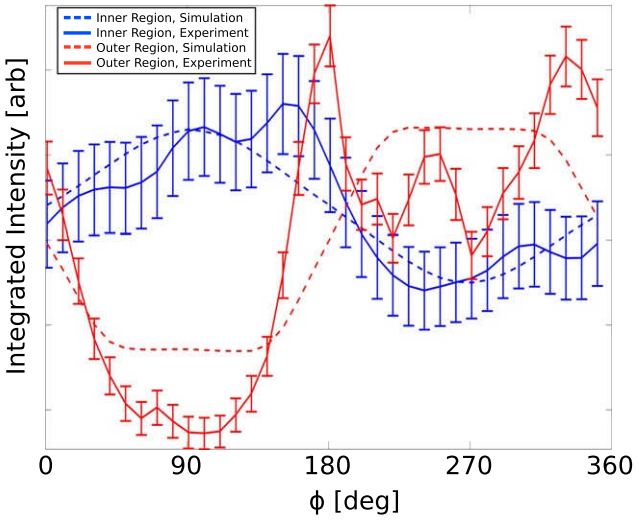


**Fig. 5.** The azimuthal variations in the integrated intensities of the observed image in Fig. 4*B*. The 2 regions of interest, the inner region and the outer region, are pictorially bounded by the red and blue circles in Fig. 4*B*. The fits (dashed lines) were computed from the simulated image of Fig. 4*B*. The one sinusoidal period is a signature of the OAM = 1 phase structure.

The triangular coils have side lengths of 8.5, 12, and 14.7 cm with an overall height of 7.3 cm. At an applied 10-A current, their inner magnetic field was $\sim$0.014 T which provided a magnetic phase gradient of $\sim 1.5\pi$ rad/mm. The triangular coils were run between 2.5 and 10 A throughout the experiment, and, in every configuration, the current in each coil was optimized to compensate for beam divergence.

The permalloy tube was built from 15 layers of a 500-$\mu$m-thick nickel–iron soft ferromagnetic sheets. The sheets were wrapped around a thin-walled aluminum pipe with an inner diameter of 3.18 cm, whose ends were cut to match the angled prism faces.

**ACKNOWLEDGMENTS.** This work was supported by the Canadian Excellence Research Chairs program, the Natural Sciences and Engineering Research Council of Canada Discovery program, Collaborative Research and Training Experience program, the Canada First Research Excellence Fund, the National Institute of Standards and Technology Quantum Information Program, the Russian Foundation for Basic Research (research project 18-29-19039), and the US Department of Energy, Office of Nuclear Physics, under Interagency Agreement 89243019SSC000025. The work utilized facilities supported, in part, by the National Science Foundation under Agreement DMR-1508249. We thank S. Watson and M. T. Hassan for their help in the experimental setup on PHADES.

1. H. Rubinsztein-Dunlop *et al.*, Roadmap on structured light. *J. Opt.* **19**, 013001 (2016).
2. S. M. Barnett, M. Babiker, M. J. Padgett, Optical orbital angular momentum. *Philos. Trans. R. Soc. A* **375**, 20150444 (2017).
3. L. Allen, M. W. Beijersbergen, R. J. C. Spreeuw, J. P. Woerdman, Orbital angular momentum of light and the transformation of Laguerre-Gaussian laser modes. *Phys. Rev. A* **45**, 8185–8189 (1992).
4. K. Y. Bliokh, Y. P. Bliokh, S. Savel'Ev, F. Nori, Semiclassical dynamics of electron wave packet states with phase vortices. *Phys. Rev. Lett.* **99**, 190404 (2007).
5. M. Uchida, A. Tonomura, Generation of electron beams carrying orbital angular momentum. *Nature* **464**, 737–739 (2010).
6. B. J. McMorran *et al.*, Electron vortex beams with high quanta of orbital angular momentum. *Science* **331**, 192–195 (2011).
7. C. W. Clark, R. Barankov, M. G. Huber, D. G. Cory, D. A. Pushin, Controlling neutron orbital angular momentum. *Nature* **525**, 504–506 (2015).
8. A. Mair, A. Vaziri, G. Weihs, A. Zeilinger, Entanglement of the orbital angular momentum states of photons. *Nature* **412**, 313–316 (2001).
9. J. Wang *et al.*, Terabit free-space data transmission employing orbital angular momentum multiplexing. *Nat. Photonics* **6**, 488–496 (2012).
10. M. F. Andersen *et al.*, Quantized rotation of atoms from photons with orbital angular momentum. *Phys. Rev. Lett.* **97**, 170406 (2006).
11. H. He, M. Friese, N. Heckenberg, H. Rubinsztein-Dunlop, Direct observation of transfer of angular momentum to absorptive particles from a laser beam with a phase singularity. *Phys. Rev. Lett.* **75**, 826–829 (1995).
12. M. Friese, J. Enger, H. Rubinsztein-Dunlop, N. R. Heckenberg, Optical angular-momentum transfer to trapped absorbing particles. *Phys. Rev. A* **54**, 1593–1596 (1996).
13. W. Brullot, M. K. Vanbel, T. Swusten, T. Verbiest, Resolving enantiomers using the optical angular momentum of twisted light. *Sci. Adv.* **2**, e1501349 (2016).
14. N. Simpson, K. Dholakia, L. Allen, M. Padgett, Mechanical equivalence of spin and orbital angular momentum of light: An optical spanner. *Opt. Lett.* **22**, 52–54 (1997).
15. R. Zhang *et al.*, Coherent optical wireless communication link employing orbital angular momentum multiplexing in a ballistic and diffusive scattering medium. *Opt. Lett.* **44**, 691–694 (2019).
16. V. Grillo *et al.*, Observation of nanoscale magnetic fields using twisted electron beams. *Nat. Commun.* **8**, 689 (2017).
17. A. Béché, R. Van Boxem, G. Van Tendeloo, J. Verbeeck, Magnetic monopole field exposed by electrons. *Nat. Phys.* **10**, 26–29 (2014).
18. D. Sarenac *et al.*, Holography with a neutron interferometer. *Opt. Express* **24**, 22528 (2016).
19. V. A. Afanasev, D. Karlovets, V. Serbo, The Schwinger scattering of twisted neutrons by nuclei. arXiv:1903.12245 (28 March 2019).
20. H. Larocque, I. Kaminer, V. Grillo, R. W. Boyd, E. Karimi, Twisting neutrons may reveal their internal structure. *Nat. Phys.* **14**, 1–2 (2018).
21. C. Maurer, A. Jesacher, S. Fürhapter, S. Bernet, M. Ritsch-Marte, Tailoring of arbitrary optical vector beams. *New J. Phys.* **9**, 78 (2007).
22. L. Marrucci, C. Manzo, D. Paparo, Optical spin-to-orbital angular momentum conversion in inhomogeneous anisotropic media. *Phys. Rev. Lett.* **96**, 163905 (2006).
23. E. Karimi, L. Marrucci, V. Grillo, E. Santamato, Spin-to-orbital angular momentum conversion and spin-polarization filtering in electron beams. *Phys. Rev. Lett.* **108**, 044801 (2012).
24. J. Nsofini *et al.*, Spin-orbit states of neutron wave packets. *Phys. Rev. A* **94**, 013605 (2016).
25. L. Marrucci *et al.*, Spin-to-orbital conversion of the angular momentum of light and its classical and quantum applications. *J. Opt.* **13**, 064001 (2011).
26. G. Milione *et al.*, $4\times$ 20 gbit/s mode division multiplexing over free space using vector modes and a q-plate mode (de) multiplexer. *Opt. Lett.* **40**, 1980–1983 (2015).
27. C. T. Schmiegelow *et al.*, Transfer of optical orbital angular momentum to a bound electron. *Nat. Commun.* **7**, 12998 (2016).
28. G. Vallone *et al.*, Free-space quantum key distribution by rotation-invariant twisted photons. *Phys. Rev. Lett.* **113**, 060503 (2014).
29. E. Karimi, V. Grillo, R. W. Boyd, E. Santamato, Generation of a spin-polarized electron beam by multipole magnetic fields. *Ultramicroscopy* **138**, 22–27 (2014).
30. K. Y. Bliokh, M. R. Dennis, F. Nori, Relativistic electron vortex beams: Angular momentum and spin-orbit interaction. *Phys. Rev. Lett.* **107**, 174802 (2011).
31. K. Y. Bliokh *et al.*, Theory and applications of free-electron vortex states. *Phys. Rep.* **690**, 1–70 (2017).
32. D. Sarenac *et al.*, Generation of a lattice of spin-orbit beams via coherent averaging. *Phys. Rev. Lett.* **121**, 183602 (2018).
33. D. Sarenac *et al.*, Methods for preparation and detection of neutron spin-orbit states. *New J. Phys.* **20**, 103012 (2018).
34. S. Tsesses *et al.*, Optical skyrmion lattice in evanescent electromagnetic fields. *Science* **361**, 993–996 (2018).
35. W. Chen *et al.*, 3He spin filter based polarized neutron capability at the NIST center for neutron research. *J. Phys. Conf. Ser.* **528**, 012014 (2014).
36. A. Abragam, *The Principles of Nuclear Magnetism* (Oxford University Press, 1961).
37. F. Li *et al.*, High resolution neutron Larmor diffraction using superconducting magnetic Wollaston prisms. *Sci. Rep.* **7**, 865 (2017).
38. W. G. Bouwman *et al.*, Real-space neutron scattering methods. *Nucl. Instrum. Methods Phys. Res. Sect. A Accel. Spectrom. Detect. Assoc. Equip.* **586**, 9–14 (2008).
39. P. J. Mohr, D. B. Newell, B. N. Taylor, Codata recommended values of the fundamental physical constants: 2014. *Rev. Mod. Phys.* **88**, 035009 (2016).
40. K. Y. Bliokh, F. Rodríguez-Fortuño, F. Nori, A. V. Zayats, Spin–orbit interactions of light. *Nat. Photonics* **9**, 796–808 (2015).
41. T. Stav *et al.*, Quantum entanglement of the spin and orbital angular momentum of photons using metamaterials. *Science* **361**, 1101–1104 (2018).
42. P. Lodahl *et al.*, Chiral quantum optics. *Nature* **541**, 473–480 (2017).
43. T. Ozawa *et al.*, Topological photonics. *Rev. Mod. Phys.* **91**, 015006 (2019).
44. NIST Center for Neutron Research, PHADES. https://ncnr.nist.gov/instruments/instdev.html. Accessed 10 April 2019.
45. M. Dietze, J. Felber, K. Raum, C. Rausch, Intensified ccds as position sensitive neutron detectors. *Nucl. Instrum. Methods Phys. Res. Sect. A Accel. Spectrom. Detect. Assoc. Equip.* **377**, 320–324 (1996).
46. W. Chen, T. Gentile, Q. Ye, T. Walker, E. Babcock, On the limits of spin-exchange optical pumping of 3He. *J. Appl. Phys.* **116**, 014903 (2014).